Chinese Chemical Letters 37 (2026) 113018

Contents lists available at ScienceDirect

Chinese Chemical Letters

journal homepage: www.elsevier.com/locate/cclet

# Atomic-level regulation of POMOF homologous isomer for photocatalytic C-H bond oxidation

Yanjie Lv[a], Xinyu Zhao[c], Jing Sun[a,*], Huiying Sun[a], Wenxi Zhang[a], Yuhan Cui[a], Xiao Li[a,*], Zhongmin Su[a,b,*]

[a] School of Chemical and Environmental Engineering, Jilin Provincial Science and Technology Innovation Centre of Optical Materials and Chemistry, Jilin Provincial International Joint Research Center of Photo-functional Materials and Chemistry, Changchun University of Science and Technology, Changchun 130022, China

[b] State Key Laboratory of Supramolecular Structure and Materials, Institute of Theoretical Chemistry, College of Chemistry, Jilin University, Changchun 130021, China

[c] Key Discipline Laboratory for National Defense for Biotechnology in Uranium Mining and Hydrometallurgy, University of South China, Hengyang 421001, China

ARTICLE INFO

*Article history:*
Received 30 March 2026
Revised 18 May 2026
Accepted 28 May 2026
Available online 29 May 2026

*Keywords:*
Hydroxide capping
Structural designation
Decatungstate
Photocatalysis
C(sp$^3$)-H oxidation

ABSTRACT

How to break through the oxidation energy barrier of C(sp$^3$)-H bonds with high dissociation energy and prevent excessive oxidation is a significant challenge. This study presents the atomic-level regulation of POMOF dimensions by inducing structural differentiation through hydroxide end-capping. Two homologous isomers, named as Co-$W_{10}$ and OH-Co-$W_{10}$ respectively, have formed three-dimensional (3D) and two-dimensional (2D) structures through varied metal coordination modes. The 2D structure of OH-Co-$W_{10}$ demonstrates excellent electron delocalization and transfer channels over the 3D structure of Co-$W_{10}$. OH-Co-$W_{10}$ exhibits enhanced oxygen activation capacity compared to Co-$W_{10}$. In the catalytic oxidation of toluene, OH-Co-$W_{10}$ achieves an impressive conversion rate of 98.1 %, and the selectivity of benzaldehyde is as high as 97.3 % (6720.2 μmol/g), which is cleaner and more efficient than that of the latest photocatalysts and Co-$W_{10}$ (4713.1 μmol/g). In this study, the hydroxide capping strategy is proposed for generation of homologous isomers, offering a new direction for catalytic oxidation of C(sp$^3$)-H bonds by expounding differences in active sites through distinct structural features.

© 2026 Published by Elsevier B.V. on behalf of Chinese Chemical Society and Institute of Materia Medica, Chinese Academy of Medical Sciences.

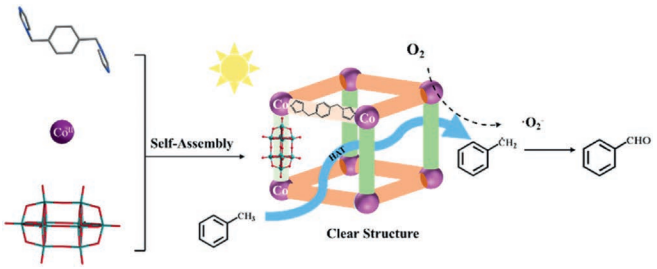
The selective oxidation of C(sp$^3$)-H bonds for alkyl aromatics synthesis driven by visible light is a crucial and the environmentally friendly way. The current significant challenge currently exists in the overcoming the oxidation energy barrier of C(sp$^3$)-H bond, while also preventing over oxidation [1–4]. A landmark example is the selective oxidation of toluene to benzaldehyde, which holds substantial industrial significance. However, benzaldehyde is highly susceptible to over oxidation, leading to the formation of benzoic acid or even extensive ring opening decomposition [5,6]. Photocatalysis utilizes light energy to activate molecular oxygen and offers a promising approach to promote selective C(sp$^3$)-H bonds oxidation under mild conditions, in which the core is the development of heterogeneous catalysts with high activity, selectivity, and stability [7–10].

In the field of photocatalytic oxidation of C(sp$^3$)-H bond, polyoxometalate-based metal-organic frameworks (POMOFs) have attracted significant attention owing to their unique electron transfer capabilities and adjustable active sites [11–13]. Clear correlation between structure and performance of POMOFs could be established through atomic level regulation of local coordination chemistry at metal nodes [14–16]. Moreover, as the structural node directly engaged in framework assembly, POMs can benefit for exposing active sites and optimizing reaction pathways directly, which requires atomic control strategies, and the selection of appropriate POMs anions to regulate coordination environment of the metal nodes.

Decatungstate ($[W_{10}O_{32}]^{4-}$, $W_{10}$) is widely used due to its unique photoactivity and hydrogen atom transfer capabilities. As a superior photosensitive unit of POMs, the electron-deficient surface of $W_{10}$ can effectively act as an oxidation center as well as broad light absorption spectrum and prolonged excited state duration [17–19]. The numerous terminal oxygen sites of $W_{10}$ can offer the potential for diverse coordination modes with metal

* Corresponding authors.
*E-mail addresses:* sj-cust@126.com (J. Sun), lix@cust.edu.cn (X. Li), zmsu@nenu.edu.cn (Z. Su).

https://doi.org/10.1016/j.cclet.2026.113018
1001-8417/© 2026 Published by Elsevier B.V. on behalf of Chinese Chemical Society and Institute of Materia Medica, Chinese Academy of Medical Sciences.




**Scheme 1.** Schematic diagram illustrating the self-assembly of POMOF building blocks and the interaction of active sites with $O_2$ and C($sp^3$)-H bonds.

ions, which make the potential candidate for POMOFs construction [20,21]. Nevertheless, how to precise control the coordination interactions of $W_{10}$-POMOFs to achieve targeted specific dimensions and pore environments, and the comprehensive elucidation of structure-activity relationship, represent significant arduous task.

In light of the aforementioned considerations, homologous isomeric POMOF systems, namely Co-$W_{10}$ and OH-Co-$W_{10}$ were designed and synthesized by self-assembly of $W_{10}$, $Co^{2+}$ and the flexible ligand bix (Scheme 1). Co-bix (the single crystal structure is shown in Fig. S1 in Supporting information), Co-$W_{10}$ and OH-Co-$W_{10}$ were applied to explore the reaction of toluene catalytic oxidation. Notably, OH-Co-$W_{10}$ exhibited superior conversion rate (98.1 %) and selectivity (97.3 %) during the oxidation of toluene to benzaldehyde. Analysis of the single crystal X-ray diffraction structure revealed that Co-$W_{10}$ structure exhibits two coordination types of cobalt sites, Co2 ($CoO_2N_4$) and Co1 ($CoN_6$) (Fig. 1a), and the OH-Co-$W_{10}$ comprises one coordination type of cobalt site, Co3 ($CoON_4(OH)$) (Fig. 1b). $W_{10}$ acts as a pillar to open the interlayer channels in the *c*-axis direction. Ligand bix adopts a trans-conformation and coordinates with Co3 and assembles in the *a*-axis direction. A hydroxide ion coordinates with one Co3 and occupies the axial position as capping agent, thereby inducing two-dimensional conjugated permeable layered structure with exposed active sites. (Fig. 1c and Fig. S3 in Supporting information). Co1 and Co2 are coordinated by $W_{10}$ and bix with conformational transformation to form a tightly packed three-dimensional framework (Fig. S2 in Supporting information). Co1 and Co2 coordinate with *cis-trans* isomers of bix, while Co3 exclusively coordinates with *trans*-bix. The *cis* conformation, characterized by tight packing and high energy, contrasts with the low-energy *trans* conformation. The 2D structure exhibits enhanced electron delocalization and transport pathways ($7.91 \times 7.54$ Å) compared to the 3D structure (Fig. S4 in Supporting information). Furthermore, the open channels in the OH-Co-$W_{10}$ structure can facilitate rapid substrate adsorption and product desorption, preventing prolonged contact and excessive oxidation risk.

The oxygen adsorption model was constructed and optimized to compare the adsorption energy of Co1, Co2 and Co3 through density functional theory (DFT) calculations. The adsorption energy (Co1 for 2.61 eV, Co2 for 0.79 eV, Co3 for -0.82 eV) gradually changed from positive to negative, and the adsorption of oxygen by the photocatalyst transformed into a spontaneous process [22–26]. The calculation results of the electron transfer quantity show that Co1 lacks a synergistic effect, and the electron transfer is restricted. In the Co-$W_{10}$ structure, Co1 is coordinated by a $CoN_6$ octahedron, and all the coordination sites are occupied by N atoms (from the bix ligand), and the electronic transfer efficiency of the ligand itself is extremely low. The $O_2$ molecule cannot directly form a chemical adsorption with Co1. The adsorption energy (+2.61 eV) is the result obtained by forcibly placing the $O_2$ molecule near Co1 and optimizing. Under the "W" synergistic effect, the electron transfer efficiency of Co2 increases. Co3 has the largest electron transfer quantity under the hydroxide electron-pushing effect and the "W" synergistic effect (Figs. 1d-f). The homogenization of Co3 coordination patterns in OH-Co-$W_{10}$ increases the density of active sites, enhances the oxygen activation efficiency, promotes the generation of superoxide radicals and singlet oxygen, and thereby improves the oxidation efficiency of toluene.

Powder X-ray diffraction (PXRD) analysis indicated that Co-bix, Co-$W_{10}$ and OH-Co-$W_{10}$ were pure phases (Figs. S5-S7 in Supporting information). In thermogravimetric analysis (TGA), Co-$W_{10}$ and OH-Co-$W_{10}$ can maintain thermal stability before 300 °C (Figs. S8 and S9 in Supporting information). For FTIR spectra, the characteristic peaks at 959.59, 887.21 and 780.52 $cm^{-1}$ are attributed to W=O, W-$O_b$-W and W-$O_c$-W, which is mainly from $W_{10}$ (Figs. S10 and S11 in Supporting information) [27]. X-ray photoelectron spectroscopy (XPS) confirmed that cobalt ions possess +2 and +3 valence states (Figs. S12 and S13 in Supporting information) [28]. The solid UV-vis spectra shows that the main absorption band of OH-Co-$W_{10}$ ($E_g = 2.84$ eV) has a significant redshift compared with Co-$W_{10}$ ($E_g = 2.96$ eV) and $W_{10}$ ($E_g = 3.05$ eV), and the reduction of the band gap proves enhanced light absorption capacity (Figs. 2a and b). Corresponding conduction band and valence band indicate that the conduction band (CB) of OH-Co-$W_{10}$ is -0.9 V (*vs.* NHE) (Figs. S14-S16 in Supporting information). The potential of $E_{CB}$ is lower than that of oxygen reduction ($O_2/\cdot O_2^-$, -0.33 V *vs.* NHE), which indicates that OH-Co-$W_{10}$ as N-type semiconductor can promote the semi-reaction of toluene oxidation. Electrochemical impedance spectroscopy (EIS) shows smaller resistance of charge transfer at the OH-Co-$W_{10}$ interface and higher carrier transfer efficiency (Fig. 2c). OH-Co-$W_{10}$ exhibits outstanding oxidation and reduction capabilities in the linear sweep voltammetry (LSV) under light irradiation (Fig. S17 in Supporting information) [29]. High transient photocurrent response intensity proves better carrier separation efficiency of OH-Co-$W_{10}$ (Fig. 2d). Photoluminescence spectroscopy and fluorescence lifetime tests showed the lifetimes of Co-$W_{10}$ and OH-Co-$W_{10}$ are 9.50 and 43.34 ns, indicating that the electron-hole recombination efficiency is lower, and catalytic reactions could occur both on the surface and channels of OH-Co-$W_{10}$ (Figs. 2e and f). Kelvin probe force microscopy (KPFM) further clarifies the dynamic process of charge transfer in photocatalysts. The carriers of N-type semiconductors are mainly electrons. In the dark state, the surface is rich in electrons. Under light conditions, the holes migrate to the surface, neutralizing some of the negative charges, resulting in positive shift in the electric potential [30–33]. By comparing the potential changes, 123 mV of OH-Co-$W_{10}$ is greater than those of Co-bix (54 mV) and Co-$W_{10}$ (108 mV). Compared with Co-bix without $W_{10}$ and tightly structured Co-$W_{10}$, the potential variation value of OH-Co-$W_{10}$ is larger, and the accumulation of surface holes is more conducive to the generation of benzyl radicals (Figs. 2g-i).

To further distinguish the contributions of coordination effect, electronic effect and geometric effect to the catalytic performance of OH-Co-$W_{10}$, a comparative analysis was conducted. Firstly, the coordination effect originated from the hydroxide end-capping on $Co^{3+}$. In OH-Co-$W_{10}$, the axial $OH^-$ ligand in the unique $CoO(N_4)(OH)$ unit has an electron-donating effect, increasing the electron density at the Co site and reducing the $O_2$ adsorption energy to -0.82 eV (spontaneous process, Fig. 1f). In contrast, Co1 ($CoN_6$) and Co2 ($CoO_2N_4$) in 3D Co-$W_{10}$ lack such end-capping groups, and their $O_2$ adsorption energies are +2.61 and +0.79 eV, respectively, indicating that the adsorption is non-spontaneous or weak adsorption. Therefore, the coordination effect is the primary factor determining the oxygen activation ability. Secondly, the electronic effect is mainly dominated by the $W_{1n}$ clusters as the photosensitizer. The narrow bandgap (2.96 eV for Co-$W_{10}$ and 2.84 eV for OH-Co-$W_{1n}$) and the lower conduction band position (-0.9

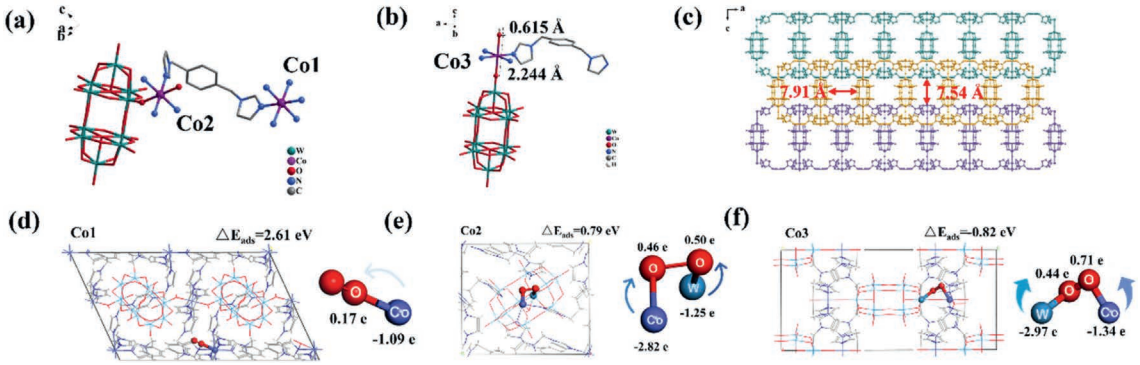



**Fig. 1.** Crystal structure diagram. (a) Asymmetric unit of Co-$W_{10}$ (The coordination modes of Co1 and Co2). (b) Asymmetric unit of OH-Co-$W_{10}$ (The coordination mode of Co3 and hydroxide). (c) The two-dimensional (2D) layered structure along the b-axis direction and the mass transfer channels of OH-Co-$W_{10}$. (d-f) The oxygen adsorption energy and electron transfer amount of Co-$W_{10}$ (Co1), Co-$W_{10}$ (Co2), OH-Co-$W_{10}$(Co3).

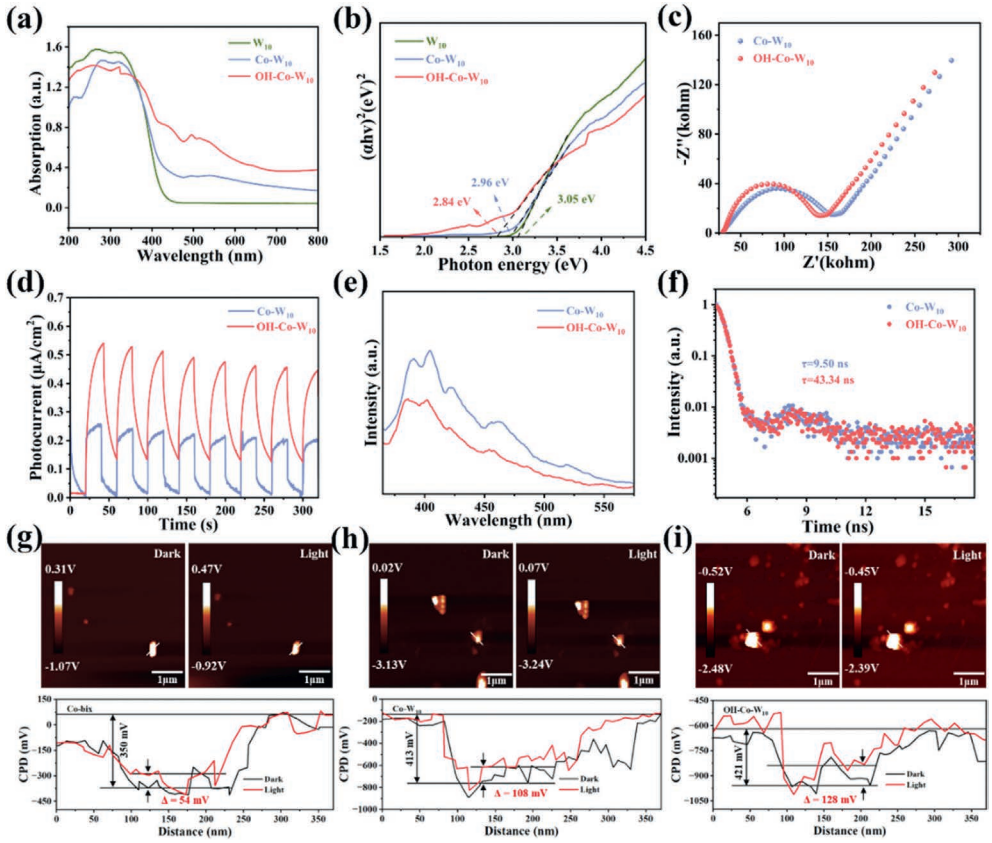



**Fig. 2.** (a) UV-vis absorption spectra. (b) Tauc plots. (c) EIS spectra. (d) Transient photocurrent response. (e) PL spectra. (f) Luminescence decay curves. KPFM images of (g) Co-bix, (h) Co-$W_{10}$, (i) OH-Co-$W_{10}$ in the dark and under light irradiation and the corresponding contact potential differences.

V *vs.* NHE) enable effective electron-hole separation under visible light. However, the electronic effect alone cannot explain the huge performance gap between the two isomers. Both materials exhibit similar transient photocurrent responses and KPFM surface potential changes (Co-$W_{10}$: 108 mV, OH-Co-$W_{10}$: 123 mV). The moderate enhancement of OH-Co-$W_{10}$ is attributed to better electron delocalization in its two-dimensional layered structure, evidenced by a longer fluorescence lifetime (43.3 ns *vs.* 9.5 ns) and a lower EIS charge transfer resistance. Finally, we found that the geometric effect is unique to the two-dimensional layered structure of OH-Co-$W_{10}$. It has open interlayer channels (7.91 × 7.54 Å), which can serve as a fast channel for substrate adsorption and product desorption. This geometric feature minimizes the residence time of benzaldehyde at the active site, thereby inhibiting the peroxidation to benzoic acid. 3D Co-$W_{10}$ has a tightly packed framework and *cis* configuration of bix ligands, lacking such accessible channels, and thus has lower selectivity.

To assess the efficiency of selective oxidation of the benzyl C($sp^3$)-H bond in aromatic compounds, Co-$W_{10}$ and OH-Co-$W_{10}$ catalysts were used as catalysts in the oxidation reaction of toluene. Employing acetonitrile as the solvent, oxygen as the oxidizing agent, and OH-Co-$W_{10}$ as the catalyst, toluene achieved a conversion rate of 98.1 %, with a benzaldehyde selectivity of 97.3 % and 2.7 % over-oxidation to benzoic acid, after 48 h of irradiation under 10 W blue LED light. Notably, OH-Co-$W_{10}$ exhibited significantly enhanced efficiency and selectivity than Co-$W_{10}$ (Fig. 3a and Fig. S18 in Supporting information). When only $W_{10}$ was present, the conversion rate and selectivity dropped significantly. The test

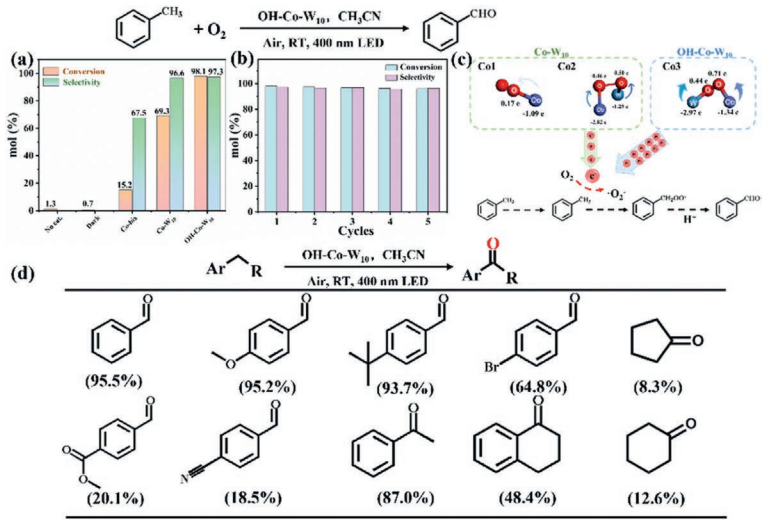



**Fig. 3.** Performance tests of the photocatalytic C($sp^3$)-H reaction. (a) Tests with different catalysts and control conditions (20 mg catalyst, 3 mL of acetonitrile, 15 μL of toluene, 100 μL of $H_2O$, 10 W 400 nm LED light). (b) Stability testing of the catalyst for five cycles. (c) Mechanism diagram of photocatalytic oxidation of toluene to benzaldehyde. (d) Substrate extension test under the same conditions.

results at other wavelengths also confirmed that 400 nm was the optimal choice (Table S6 in Supporting information). The results of molecular dynamics show that the catalytic oxidation reaction of toluene by OH-Co-$W_{10}$ mainly occurs within the 2D confined pores (Fig. S19 in Supporting information). Only a trace amount of toluene conversion rate was observed when no light and catalyst (Fig. 3a), which further highlights the significance of catalysts and light in the photocatalytic oxidation process of toluene. The design of metal coordination modes and dimensional variance have endowed OH-Co-$W_{10}$ with stronger capability in catalyzing surface oxidation reactions comprehensively. Furthermore, the transport channels of OH-Co-$W_{10}$ promote rapid substrate adsorption and product desorption, thereby strengthening the selectivity of benzaldehyde.

Recyclability, stability and high efficiency are of vital importance for heterogeneous catalysts [34–36]. After five cycles of recycling and reutilization, OH-Co-$W_{10}$ exhibited only slight decrease in both conversion rate and selectivity (Fig. 3b). Noteworthy, the PXRD and FTIR analyses revealed no significant alterations in the structures before and after the reaction, proving the effectiveness of Co-$W_{10}$ and OH-Co-$W_{10}$ as heterogeneous catalysts (Figs. S20-S22 in Supporting information). To clarify the reactive oxygen species (ROS), free radical capture experiments and electron paramagnetic resonance (EPR) tests were conducted utilizing various quenchers (Table S7 and Fig. S23 in Supporting information). The inclusion of $AgNO_3$ notably decreased the yield of toluene oxidation, indicating the involvement of electron transfer (ET) in this process [37–40]. According to the results of density functional theory (DFT) calculations, both W and Co in the Co-$W_{10}$ and OH-Co-$W_{10}$ structures can transfer electrons to $O_2$. Among them, a certain type of Co3 in OH-Co-$W_{10}$ has a higher electron transfer efficiency compared to Co1 and Co2 in Co-$W_{10}$, which have very low electron transfer amounts. Based on the amount of electron transfer and whether the adsorption occurs spontaneously, it can be determined that OH-Co-$W_{10}$ has a higher oxygen activation ability. This is also an important reason why OH-Co-$W_{10}$ has a higher conversion rate in the toluene oxidation reaction. Furthermore, the introduction of *p*-benzoquinone (scavengers of $\cdot O_2^-$) resulted in a decrease in the conversion rate, suggesting the potential significance of $\cdot O_2^-$ as reactive oxygen species for OH-Co-$W_{10}$ activation (Fig. 3c). As an n-type semiconductor, Co-$W_{10}$ and OH-Co-$W_{10}$ have narrow band gap and generates electrons and holes ($h^+$) under illumination. In the subsequent reaction, the photogenerated electrons reduce $O_2$ to $\cdot O_2^-$ radicals, while the holes activate toluene to form cationic radicals. These radicals then react with $\cdot O_2^-$ radicals and $O_2$ to form benzaldehyde.

A key mechanistic question is whether the electron transfer (ET) pathway is mutually exclusive with the classical hydrogen atom transfer (HAT) mechanism known for decatungstate photocatalysts. In this POMOF systems, the two pathways are not mutually exclusive but operate synergistically. The $W_{10}$ unit retains its intrinsic HAT activity, as confirmed by the TBADT control experiment (Table S6). Meanwhile, the Co centers act as electron relays, enabling an ET pathway, photogenerated electrons are transferred from $W_{10}$ to Co and then to $O_2$, generating $\cdot O_2^-$, while the remaining holes oxidize toluene to the benzyl radical. This hybrid mechanism is supported by DFT, KPFM and scavenger experiments. The Co centers, particularly Co3 with the $OH^-$ ligand, play a crucial role in facilitating $O_2$ activation and mediating electron transfer, thereby enhancing both activity and selectivity.

When toluene is oxidized in solvents of different polarities, both the conversion rate and selectivity will decrease to varying degrees (Table S8 in Supporting information). This is mainly because a high dielectric constant enhances the separation of photogenerated electrons and holes, reducing the probability of recombination [41–45]. In addition, during the substrate expansion experiment test, methylbenzene with substitution can also be oxidized into the corresponding aldehyde. Among them, electron-donating groups promote the high selectivity of aldehydes. Other substituents produce carbonyl compounds also exhibit high selectivity (Fig. 3d). The efficiency and perfect selectivity of OH-Co-$W_{10}$ in the oxidation of toluene are comparable to those of most reported catalysts (Tables S9 and S10 in Supporting information).

In summary, we constructed two homologous heterogeneous POMOF systems (Co-$W_{10}$ and OH-Co-$W_{10}$) using the hydroxide end-capping strategy. By systematically distributing steric, electronic, and geometric effects, we revealed that the $OH^-$ end-capping ligand achieved spontaneous $O_2$ adsorption and activation through the coordination effect on $Co^{3+}$. At the same time, the electronic effect of the $W_{10}$ photosensitizer provided efficient charge separation, and the two-dimensional layered structure further enhanced electron delocalization. Additionally, the geometric effect of the two-dimensional open channels promoted the rapid desorption of products and inhibited peroxidation, thereby achiev-

ing 97.3 % selectivity for benzaldehyde. This work not only provides an efficient catalyst for C($sp^3$)-H bond oxidation, but also establishes a clear framework for distinguishing various structural effects in POMOF design.

## CRediT authorship contribution statement

**Yanjie Lv:** Writing – original draft, Methodology, Investigation, Conceptualization. **Xinyu Zhao:** Methodology, Investigation. **Jing Sun:** Writing – review & editing, Supervision, Funding acquisition. **Huiying Sun:** Software, Funding acquisition. **Wenxi Zhang:** Investigation. **Yuhan Cui:** Investigation. **Xiao Li:** Writing – review & editing, Supervision. **Zhongmin Su:** Writing – review & editing, Supervision, Funding acquisition.

## Declaration of competing interest

The authors declare that they have no known competing financial interests or personal relationships that could have appeared to influence the work reported in this paper.

## Acknowledgments

This work was financially supported by the National Natural Science Foundation of China (No. 22271023), Natural Science Foundation of Jilin Province Science and Technology Department (General Project of Free Exploration, No. YDZJ202401564ZYTS), the Science and Technology Research Project of Jilin Provincial Department of Education (No. JJKH20240899KJ).

## Supplementary materials

Supplementary material associated with this article can be found, in the online version, at doi:10.1016/j.cclet.2026.113018.

## References

[1] Q. Shen, J. Chen, X. Jing, C. Duan, Angew. Chem. Int. Ed. 64 (2025) e202506277.
[2] Y. Yang, X.H. Yang, L.G. Tang, et al., Adv. Mater. 37 (2025) 2502321.
[3] C. Ma, C. Yang, H. Zhuo, et al., J. Am. Chem. Soc. 145 (2023) 10890–10898.
[4] M. Zhang, Y. Li, R.K. Gupta, Chin. Chem. Lett. (2025), doi:10.1016/j.cclet.2025.111897.
[5] W. Qiao, X. Fan, W.F. Liu, et al., J. Am. Chem. Soc. 145 (2023) 5353–5362.
[6] T.X. Luan, L.B. Xing, N. Lu, et al., J. Am. Chem. Soc. 147 (2025) 12704–12714.
[7] M. Wu, S. Mushina, M. Tan, Chin. Chem. Lett. 37 (2026) 111923.
[8] Y. Xu, Y. Lin, S.L. Homölle, et al., J. Am. Chem. Soc. 146 (2024) 24105–24113.
[9] Y. Teng, Z. Zhou, J. Chen, Chin. Chem. Lett. 36 (2025) 110430.
[10] H.F. Zheng, Y.J. Fan, A.L. Blenko, et al., J. Am. Chem. Soc. 145 (2023) 9994–10000.
[11] Y. Liu, C.S. Tang, M. Cheng, et al., ACS Catal. 11 (2021) 13374–13396.
[12] A. Solé-Daura, Y. Benseghir, M.H. Ha-Thi, et al., ACS Catal. 12 (2022) 9244–9255.
[13] X.H. Liu, H. Li, N. Xu, et al., Chin. J. Chem. 42 (2024) 2970–2978.
[14] T. Zhang, J.C. Jiao, K.X. Guo, et al., J. Catal. 436 (2024) 115637.
[15] G. Ji, L. Zhao, Y. Wang, et al., ACS Catal. 12 (2022) 7821–7832.
[16] D. Nowicka, N. Vadra, E. Wieczorek-Szweda, et al., Coordin. Chem. Rev. 519 (2024) 216091.
[17] K. Sheng, Z. Wang, L. Li, et al., J. Am. Chem. Soc. 145 (2023) 10595–10603.
[18] J. Zhang, A. Studer, Nat. Commun. 13 (2022) 3886.
[19] I.B. Perry, T.F. Brewer, P.J. Sarver, et al., Nature 560 (2018) 70–75.
[20] X. Yan, J. Xu, T. Zhang, et al., Chin. Chem. Lett. 34 (2023) 107851.
[21] D.Y. Du, J.S. Qin, S.L. Li, et al., Chem. Soc. Rev. 43 (2014) 4615–4632.
[22] L.Y. Meng, Y.J. Dong, B. Zhu, et al., Dalton Trans. 51 (2022) 7928–7935.
[23] X. Song, C. Jin, H. Chen, et al., CCS Chem. 6 (2024) 208–217.
[24] J. Li, X. Luo, Y. Zhou, et al., Cryst. Growth Des. 18 (2018) 1857–1863.
[25] M.Y. Chen, Q.Y. Li, X.Y. Xu, et al., Chem. Eng. J. 494 (2024) 153133.
[26] H.Y. Sun, Z.L. Lang, Y.N. Zhao, et al., Angew. Chem. Int. Ed. 61 (2022) e202202914.
[27] S.Q. You, Y.J. Dong, B.S. Hou, et al., J. Mater. Chem. C 11 (2023) 7389–7396.
[28] T. Zhang, Ji.C. Jiao, K.X. Guo, et al., J. Catal. 429 (2024) 115287.
[29] X.Y. Chu, S.K. Liu, B.B. Luan, et al., Angew. Chem. Int. Ed. 64 (2025) e202422940.
[30] C.Y. Pan, K.G. Huang, Z.H. Zhi, et al., Adv. Energy Mater. 16 (2026) 2405708.
[31] M.J. Guo, A. Talebian-Kiakalaieh, E.M. Hashem, et al., Adv. Funct. Mater. 34 (2024) 2406356.
[32] A. Zahmatkeshsaredorahi, R. Millan-Solsona, D.S. Jakob, L. Collins, X.G. Xu, Nat. Rev. Method. Prime. 5 (2025) 53.
[33] D.S. Jakob, H. Wang, G. Zeng, et al., Angew. Chem. 132 (2020) 16217–16224.
[34] D.J. Cao, C.T. Gong, Y.K. Han, et al., Angew. Chem. Int. Ed. 64 (2025) e202516908.
[35] B. Chen, B. Li, Y. Su, et al., Angew. Chem. Int. Ed. 64 (2025) e202515924.
[36] M. Cui, D. Wang, J. Guo, et al., J. Am. Chem. Soc. 147 (2025) 32982–32993.
[37] J.J. Li, J.Y. Liu, S.Y. Gao, X. Yang, R. Cao, J. Am. Chem. Soc. 147 (2025) 21754–21763.
[38] Y.J. Lv, D.X. Peng, W.X. Zhang, et al., J. Catal. 446 (2025) 116088.
[39] M. Moreno-Albarracín, A.M. Rodriguez-Jimenez, O. Nuñez, P. Garrido-Barros, Angew. Chem. Int. Ed. 64 (2025) e202510723.
[40] G. Li, P. Fu, Q. Yue, et al., Chem Catal. 2 (2022) 1734–1747.
[41] X. Wu, S. Xie, D. Vangestel, H. Zhao, B. Sels, Angew. Chem. Int. Ed. 63 (2024) e202409826.
[42] G. Zhang, Y. Xu, P. Zhang, C. He, H. Mi, ACS Nano 18 (2024) 29294–29303.
[43] S. Guo, L.H. Kong, P. Wang, et al., Angew. Chem. Int. Ed. 61 (2022) e202206193.
[44] S. Fu, S. Yao, S. Guo, et al., J. Am. Chem. Soc. 143 (2021) 20792–20801.
[45] K. Chen, S. Guo, H. Liu, et al., Angew. Chem. Int. Ed. 59 (2020) 12951–12957.